Investigation of spin reorientation and magnetocaloric behavior in PrCo 5 – x Cu x compounds

H. Jaballah, V. Charbonnier, Lotfi Bessais, N. Mliki

Investigation of Spin Reorientation and Magnetocaloric Behavior in $PrCo_{5-x}Cu_x$ Compounds

H. Jaballah,[1,2] V. Charbonnier,[3] L. Bessais,[2] and N. Mliki[1]

[1] *Université de Tunis El Manar, Faculté des Sciences de Tunis, Laboratoire Matériaux Organisation et Propriétés, Tunis 2092, Tunisia.*

[2] *Univ Paris Est Creteil, CNRS, ICMPE, UMR 7182, 2 rue Henri Dunant, F-94320 Thiais, France*

[3] *Energy Process Research Institute, National Institute of Advanced Industrial Science and Technology (AIST), Tsukuba West, 16-1 Onogawa, Tsukuba, Ibaraki, 305-8569, Japan*

(Dated: May 1, 2024)

In the present work, we have studied the structural and magnetic properties of the compounds $PrCo_2Cu_3$, $PrCo_{2.5}Cu_{2.5}$ and $PrCo_3Cu_2$ as well as **their spin reorientation transition and magnetocaloric behavior**. All three compounds crystallize in the hexagonal $CaCu_5$-type structure. The lattice parameters increase when copper replaces cobalt. The temperature dependence of the magnetization has been determined at low and high temperatures. It revealed that the Curie temperature decreases from $\sim$ 1000 K to 310 K after the substitution of cobalt by copper ($PrCo_2Cu_3$). For the copper-rich compound, a merging of the transition from the planar ferromagnetic state to the axial ferromagnetic one and the transition from the ferromagnetic state to the paramagnetic one is observed. A constant entropy variation is observed over a wide temperature range centered around room temperature. It results from the merging of the entropy measured around the spin reorientation temperature and that measured around Curie temperature.

PACS numbers: 75.50.Bb, 75.50.Tt, 76.80.+y
Keywords: Intermetallic rare-earth transition-metal compounds; Magnetic materials; Magnetocaloric Effect.

I. INTRODUCTION

Due to their interesting performances in terms of magnetic properties, a particular interest has been given to the study of compounds based on rare earth elements (R) and 3*d* transition metals (T). The origin of the exceptional magnetic properties of compounds based on R-T intermetallics is the coexistence of two complementary types of magnetism: the localized magnetism of rare earths and the itinerant magnetism of 3*d* transition metals. They are interesting for several applications. Among them, we may cite the high-density magnetic recording (Sm_2Co_{17}−Cu [1], and TbFeCo [2]), the hard magnets (SmCo, NdFeB, and PrCo [3–6]), and the magnetic refrigeration ($Gd_5(Ge,Si)_4$ and $La(Fe,Co,Si)_{13}(H,C)$). R-T binary systems have been the subject of numerous systematic research in order to determine the existing compounds, their range of stability and their crystallographic structure. The most studied stoichiometry in R-T binary systems is RT_5. Two main motivations can explain this. First of all, in these phases, R and T can be substituted by other rare earth elements and 3*d* transition metals. This provides a wide range of possibilities for tuning the composition and thereby the properties of the resulting compound. Second, these phases are the base for the formation of other intermetallic compounds based on rare-earth elements and 3*d* transition metals.

According to the literature, it is clear that the studies carried out on RT_5 intermetallic compounds have been concentrated on the optimization of the anisotropy field, the coercive field and microstructure for permanent magnet application [7–10]. Another potential application of RT_5 is magnetic cooling, which is based on the magnetocaloric effect (MCE).

The magnetocaloric effect is a characteristic of paramagnetic and ferromagnetic materials where there is a rise in temperature when exposed to changes in magnetic field in adiabatic conditions; whereas a cooling effect arises when the material is demagnetized [11]. MCE reaches its maximum around the Curie temperature in the case of ferromagnetic materials. It is well known that intermetallic RT_5 have very high Curie temperatures. Therefore, it is necessary to decrease the value of T_C in order to have the maximum of the magnetocaloric effect around the room temperature.

The aim of this study is to obtain a pure $PrCo_5$ phase and to lower its Curie temperature from $\sim$1000 K to a value close to room temperature. For this purpose, there are two alternatives: performing a substitution either in the site of rare earth atoms or in the site of transition metal atoms. Substitution in the rare earth site is relatively difficult due to the volatile nature of rare earths and their rapid oxidation upon contact with air. On top of that, since praseodymium has a low de Gennes factor, the range of variation of the T_C value as a function of the concentration of the substituent will be narrow. A alternative is the substitution in the transition metal site. The transition metal atom (T) must fulfill two criteria: the transition metal should form a stable $Pr(Co,T)_5$ phase and T must have a magnetic moment zero or lower than cobalt. For the binary $PrCo_5$, copper fulfills the two previous criteria. In this paper, we present the effect of copper on the structure, thermomagnetic properties and advantage of the anisotropy change phenomenon in the magnetocaloric effect around room temperature.

II. EXPERIMENTAL METHODS

$PrCo_{5-x}Cu_x$ compounds have been prepared from high purity elements cobalt (99.98%), copper (99.98%) and praseodymium (99.98%) by arc-melting technique under a purified argon atmosphere. The elements are placed in a copper crucible cooled by cold water. After ingot formation, the compound is wrapped in tantalum foil and introduced into a silica tube sealed under secondary vacuum 2×10^{-6} bar [12–14]. The ingot has been heat-treated for seven days at 1223 K, and was finally, water quenched [15–17].

Phase analysis has been performed on powder by X-ray powder diffraction (XRD). A D8 Brucker diffractometer with Cu Kα radiation $\lambda = 1.54178$ Å was used. XRD data of the samples have been collected between 20 and 80° at room temperature with 0.015° step width.

XRD diagrams are analyzed with the Rietveld method [18, 19] using the FullProf program [20, 21]. The peak shape function has been selected as Thompson-Cox-Hastings pseudo-Voigt type [22]. The goodness of fit indicators R_B and χ^2 are calculated from the program output to measure the quality of refinement, and they are defined as:

$$R_B = 100 \frac{\sum_K |I_K(O) - I_K(C)|}{\sum_K I_K(O)}$$

and

$$\chi^2 = \frac{\sum_i w_i |y_i(O) - y_i(C)|}{N - P}$$

where $I_K(O)$ is the observed Bragg intensity and $I_K(C)$ is the calculated one. $y_i(O)$ is the intensity observed at the i^{th} step in the step scanned powder diffraction pattern, $y_i(C)$ is that calculated, and w_i is the weight of the observation. N is the total number of points used in the refinement and P the number of refined parameters.

The refined parameters are unit cell parameters, scale factors U, V, W, background points, and atomic positions [5, 23–25]. To refine the structure of the studied samples, the input atomic parameters have been taken from Refs. [26–28].

Magnetic properties are measured using a magneto/susceptometer Manics DSM8 operating on the same principle as a Faraday type balance between 300 and 900 K [29]. A Physical Properties Measurement System (PPMS) magnetometer is used for measurements at low temperatures between 70 and 330 K. Recently it has been reported that, the demagnetizing field might have a notable influence on the result of magnetocaloric effect [30]. The following equation was used to get the internal field (H_int):

$$H_{int} = H_{ext} - N_{Demag} M(T, H_{ext})$$

M is the measured magnetization, H_{ext} is the external applied magnetic field (non corrected field) that should be corrected to take into account the demagnetization effect. Demagnetization constant N_{Demag} has been determined from M vs H_{ext} curve in a low field region following the method given in Ref. [31]. The corrected magnetic field H_{int} has been used for the present magnetic results.

III. RESULTS AND DISCUSSION

A. Structure analysis

Fig. 1(a) shows the XRD diffractograms of the alloys $Pr(Co,Cu)_5$ for (x = 2, 2.5, 3).The compounds are single phase and crystallize into the hexagonal $CaCu_5$-type structure with $P6/mmm$ space group. We note that Cu atoms replace Co atoms without any change in the structure. However, by increasing the Cu content, a progressive shift of the peaks to smaller diffraction angles occurs. It indicates the increase of the cell volume and is due to the difference between the atomic radii of Cu and Co atoms.

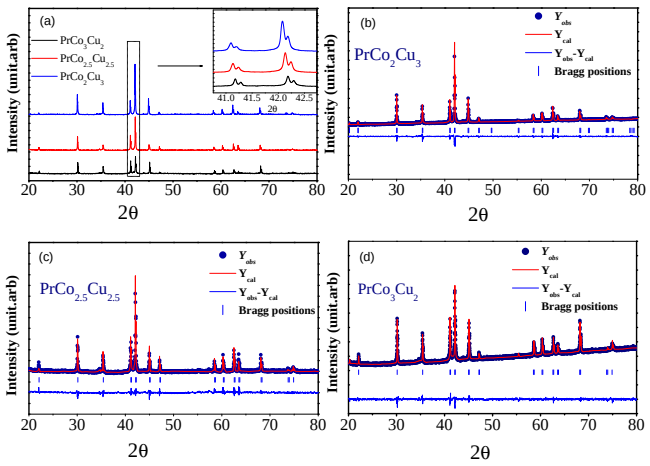

Figure 1. **(a) XRD diffractograms of the bulk alloys for $PrCo_2Cu_3$, $PrCo_{2.5}Cu_{2.5}$ and $PrCo_3Cu_2$ compounds. Rietveld refinement pattern of XRD data for $PrCo_2Cu_3$ (b), $PrCo_{2.5}Cu_{2.5}$ (c) and $PrCo_3Cu_2$ (d) compounds. The blue circles and red line present respectively the experimental intensities and the calculated intensities. The blue vertical bars correspond to (hkl) line positions (Positions of Bragg peaks). The blue line shows the difference between the calculated and experimental intensities.**

The XRD diagrams of the compounds $PrCo_2Cu_3$, $PrCo_{2.5}Cu_{2.5}$ and $PrCo_3Cu_2$ are presented with their Rietveld refinements in Fig. 1(b), (c) and (d). The pure $PrCo_5$ compound crystallizes in a hexagonal $CaCu_5$-type structure in the $P6/mmm$ space group [32]. In this structure, Pr atoms occupy the 1a sites, while Co atoms

occupy two different crystallographic sites: $3g$ and $2c$ (in Wyckoff notation). The Rietveld refinement confirms that the compounds $PrCo_2Cu_3$, $PrCo_{2.5}Cu_{2.5}$ and $PrCo_3Cu_2$ crystallize in the same space group as $PrCo_5$ ($P6/mmm$). The atomic, structural parameters and agreement factors (R_B and χ^2) are listed in Table. I.

We performed several refinements trying to distribute the copper atoms over the two cobalt sites $2c$ and $3g$, while respecting the nominal composition of each sample. The best agreement factor R_B obtained corresponds to the substitution of cobalt by copper at the $3g$ site for all three samples. When copper occupies the other site $2c$, we notice a deterioration of χ^2 (goodness of fit). This can be explained by the difference in size between Co and Cu. Indeed, the radius of the Cu is slightly larger than that of Co. This is why Cu prefers the $3g$ site which has a larger volume than the $2c$ site.

Table I. a and c unit cell parameters, R_B, χ^2 factors, and atomic positions from Rietveld refinement of $PrCo_{5-x}Cu_x$.

	$x=2$	$x=2.5$	$x=3$
a (Å)	5.0643(6)	5.0710 (9)	5.0753 (5)
c (Å)	4.0187(8)	4.0293 (7)	4.0388 (3)
c/a	0.7935(3)	0.7945(3)	0.7957 (4)
V (Å^3)	89.265	89.733	90.098
χ^2	3.89	4.15	3.71
R_B	9.64	9.35	5.25
Preferential site for Cu	$3g$	$3g$	$3g$

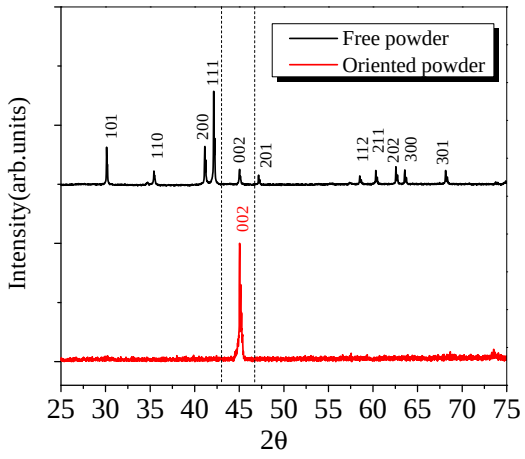

Figure 2. X-ray diffraction of free and oriented powder for $PrCo_3Cu_2$ compound.

Table. I shows that after the partial substitution of cobalt by copper, there is an increase in the cell parameters a, c and V. For $x=2$, a and c are respectively 5.0643(6) and 4.0187(8) Å. Similar cell parameter values and atom positions have been found in previous work [8]. For $x=3$, a and c are 5.0753(5) and 4.0388(3)Å, respectively. The cell volume increases slightly from 89.265 Å^3 to 90.098 Å^3 as well as the ratio c/a. The increase of the c/a ratio shows that the expansion of the lattice occurs in an anisotropic way.

The RCo_5 compounds show a significant uniaxial magneto-crystalline anisotropy; it results from the anisotropies contributed by the R atom. Figure 2 shows the comparison between the X-ray diffractograms of the free powder and the oriented powder measured at 300 K on $PrCo_3Cu_2$. The XRD obtained on the oriented powders shows a disappearance of some reticular planes and the strengthening of the $(00l)$ indexed Bragg peaks compared to the diagram measured on the free powder; thus, the axis of easy magnetization at room temperature is the c-axis. This magnetic anisotropy is clearly evidenced by the strengthening of the (002) Bragg peak. The same results are obtained for the two other compositions.

B. Magnetic properties

1. *Thermomagnetic properties*

a. ***Curie temperature:*** The variation of magnetization against temperature under an applied magnetic field equal to 50 mT for samples sealed under secondary vacuum is shown in Fig. 3. It shows an abrupt drop in magnetization, signature of a phase transition from a ferromagnetic to a paramagnetic state. The Curie temperature T_C is determined by the first derivative of $M(T)$. The value of the Curie temperature corresponds to the minimum of the derivative of the magnetization curve.

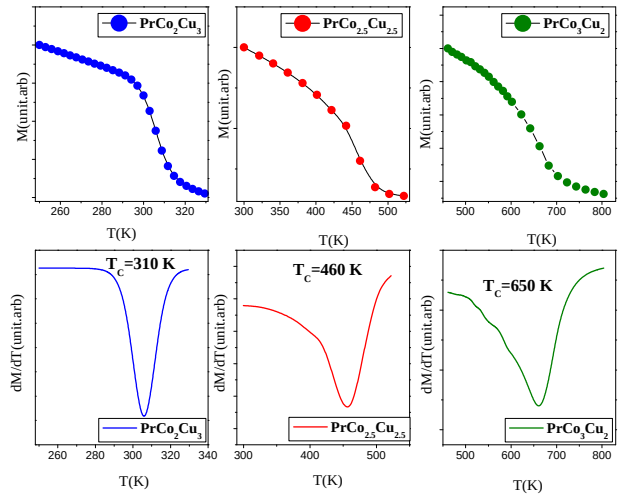

Figure 3. Magnetization plotted versus temperature for $PrCo_2Cu_3$, $PrCo_{2.5}Cu_{2.5}$ and $PrCo_3Cu_2$ compounds, under low applied magnetic field equal to 50 mT.

The evolution of T_C as a function of the Cu content is shown in Tab. II. T_C decreases significantly after the sub-

stitution of the Co atom by the Cu atom. The value of T_C for the compound $Pr(Co,Cu)_5$ decreases with increasing copper concentration, for $x = 2, 2.5$ and 3, the values of T_C are equal to 650 K, 460 K and 310 K, respectively.

Table II. Curie temperature values as a function of copper content for $PrCo_{5-x}Cu_x$

$PrCo_{5-x}Cu_x$	x=0	x=2	x=2.5	x=3
T_C (K)	912 [33]	650	460	310

In the general case, the Curie temperature is governed by the exchange interactions. In the case of an R-T intermetallic compound, there are three types of exchange interactions: the exchange interaction between the magnetic moments of the transition metal atoms ($3d$–$3d$), the exchange interaction between the magnetic moments of the rare earth atoms ($4f$–$4f$), and the exchange interaction between the two sublattices ($3d$–$4f$).

Among these three configurations, the $4f$–$4f$ exchange interaction is the weakest. Similarly, we can neglect the $3d$–$4f$ exchange. Therefore, only the interaction between the $3d$–$3d$ transition metal magnetic moments contributes to the Curie temperature. In this case, only the $3d$–$3d$ exchange interaction will be considered. Note that there are two types of $3d$–$3d$ exchange interactions in intermetallics, positive and negative. In the case where the interatomic distance (T–T) is less than a certain critical distance (2.45 Å), the exchange interactions are negative; otherwise, they are positive [34]. The Rietveld refinement results show a very small volume change, and actually, the T–T distances did not vary significantly.

Another important factor responsible for the increase of T_C is the electronic effect. In fact, the copper atom has two extra electrons compared to the cobalt atom, the two extra electrons of Cu can fill the $3d$ band, consequently the $3d$ band becomes more symmetrical which results in a decrease of cobalt magnetic moment. In the end, the decrease of T_C can be explained by the magnetic dilution due to the substitution of an atom with high magnetic moment (Co) by a non-magnetic atom (Cu) with larger number of electrons.

b. ***Spin-reorientation transitions:*** The spin reorientation transition is a magnetic transition accompanied by a change of magneto-crystalline anisotropy, in other words, a change of easy magnetization direction, this transition can be observed in anisotropic magnetic materials that present at least two sublattices favoring two different competitive easy magnetization directions. The compositions we present in this study include a rare earth atom (Pr) with an electronic shell $4f$ flattened perpendicular to the direction of the moment, this favors a planar anisotropy. Moreover, the compounds contain cobalt which favors an axial anisotropy. Since the above mentioned transition is accompanied by a magnetization variation, we present in this section the results of magnetization measurements at low temperature, in the following we explain with more details the observed phenomenon. Thus, the effect of this transition on the magnetic entropy variation is presented, because of the importance of this quantity on the evaluation of magnetocaloric materials.

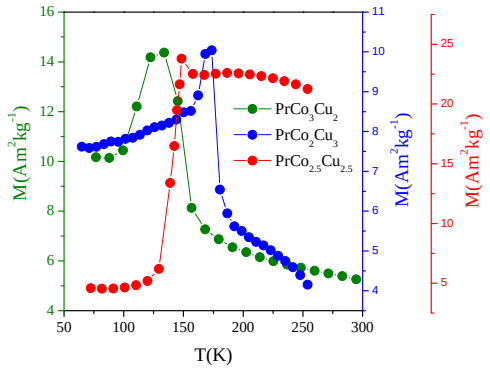

Figure 4. Magnetization plotted against temperature for $PrCo_2Cu_3$, $PrCo_{2.5}Cu_{2.5}$ and $PrCo_3Cu_2$ compounds at low temperature, under low applied magnetic field equal to 50 mT.

Fig. 4 shows the variation of magnetization as a function of temperature between 77 K and 300 K for the compounds $PrCo_{5-x}Cu_x$ ($x = 2, 2.5, 3$) measured under an applied magnetic field equal to H_{ext}=50 mT. For the three compositions a jump in the magnetization value is observed. The temperature corresponding to the observed maxima increases with the increase of the copper content. The sharpest peak is observed for the compound $PrCo_2Cu_3$.

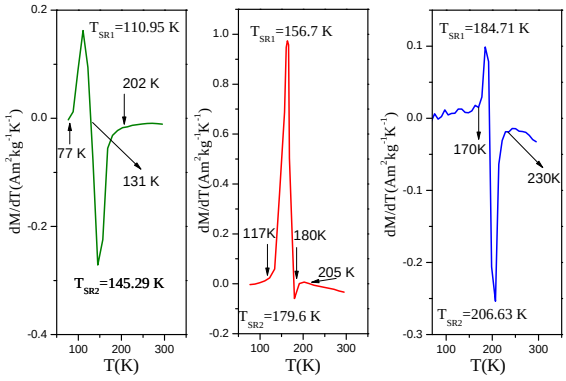

Figure 5. Derivation of magnetization plotted against temperature for $PrCo_2Cu_3$ (right), $PrCo_{2.5}Cu_{2.5}$ (middle) and $PrCo_3Cu_2$ (left) compounds at low temperature, under low applied magnetic field equal to 50 mT.

Fig. 5 shows the magnetization derivative for the compounds $PrCo_{5-x}Cu_x$ derived from Fig. 4. All the derivative curves have two extrema. For $x = 2$ and $x = 3$ the second extremum (minimum) is higher than the first extremum (maximum), on the other hand, for $x = 2.5$ the

maximum is higher than the minimum. The highest extremum for the three compositions is the one corresponding to the maximum of the magnetization derivative for a copper concentration equal to $x = 2.5$.

The anisotropy of the rare-earths is imposed by the shape of the magnetic $4f$ electron band, such that rare-earths with a positive second-order Steven coefficient α_j (Er and Sm) exhibit axial anisotropy along the c-axis and, therefore, enhance the anisotropy of the Co sublattice that is also along the c-axis. On the other hand, rare earths with $\alpha_j \leq 0$ (Pr, Nd, Tb, Dy and Ho) tend to have an easy magnetization direction in the basal $a-b$ plane of the hexagonal structure [35]. In the latter case, we have a coexistence of these two competing anisotropies, which are: axial for the Co sublattice and planar $a-b$ for the rare earth sublattice [36]. This competition induces a spin reorientation phenomenon in these compounds and governs some magnetic properties.

For temperatures below transition temperature from the planar ferromagnetic state to the conical ferromagnetic state (T_{SR1}), the anisotropy of the Pr sublattice is larger than that of the Co sublattice and, consequently, the total magnetic moment lies in the basal $a-b$ plane. Note that, in this case, the magnetic moments of Pr and Co are collinear [36]. On the other hand, for a temperature higher than transition temperature from the conical ferromagnetic state to the axial ferromagnetic state T_{SR2}, the anisotropy of the Co sublattice is higher than that of the other sublattices, therefore, the basal plane becomes the hard plane and the c-axis becomes the easy magnetization direction. Again, in this case, the two magnetic moments are collinear [36].

For a temperature value between T_{SR1} and T_{SR2}, there is a strong competition between the magnetocrystalline anisotropy magnetic moments of the two sublattices Pr and Co and, as a consequence, the total magnetic moment takes a conical arrangement between the basal plane and the c-axis. In a different way than before, the magnetic moment of these sublattices is non-collinear [36] for temperatures between T_{SR1} and T_{SR2}. Thus, the spin reorientation process occurs in a temperature range between T_{SR1} and T_{SR2} [36] rather than at a specific temperature. Measurements of magnetization as a function of temperature elucidate the above discussion; T_{SR1} and T_{SR2} correspond to the first and second inflection points of the $M(T)$ curves, as shown in Fig. 5 for samples with $x = 2$, 2.5, and 3. **Upon examining the magnetic properties of the three compounds, it can be seen that the spin reorientation transition in the compound with $x = 2.5$ exhibits a pronounced distinction compared to the other two compounds. Specifically, the transition from the conical ferromagnetic state to the axial ferromagnetic state is less evident. To clarify this particular behavior, we plan to perform neutron diffraction and Monte-Carlo simulations.**

From the magnetization curves, we show a schematic magnetic phase diagram for this $PrCo_{5-x}Cu_x$ series, as presented in Fig. 6. For low temperatures, the total magnetic moment lies in the $a-b$ plane. For a given composition, the axis of easy magnetization changes direction with increasing temperature, but the system state remains ferromagnetic, further increasing the temperature a phase transition from ferromagnetic to paramagnetic state is observed. As the copper concentration increases, the spin reorientation temperature increases and the Curie temperature decreases. The decrease of the Curie temperature is due to the magnetic dilution following the substitution of cobalt by copper. The increase of the spin reorientation temperature with the copper concentration is explained by the fact that the axial anisotropy becomes less favored when the cobalt content decreases.

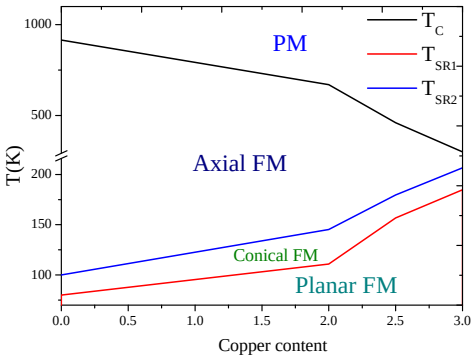

Figure 6. Schematic magnetic phase diagram for $PrCo_{5-x}Cu_x$ compounds. FM and PM mean ferromagnetic and paramagnetic state, respectively. Curie temperature of $PrCo_5$ is taken from Ref. [33]

2. *Critical behavior around room temperature*

In this section, our focus is solely on investigating the ferromagnetic-paramagnetic (FM-PM) phase transition of $PrCo_2Cu_3$, for two primary reasons. Firstly, the FM-PM transition occurs at room temperature, unlike the other two compositions where the Curie temperatures are high. Secondly, the $PrCo_2Cu_3$ compound boasts the narrowest temperature interval between the ferromagnetic-paramagnetic phase transition and the spin reorientation transition. Therefore, a comprehensive analysis of the critical behavior exhibited during the FM-PM transition is crucial to gain a deeper understanding of the magnetic properties of $PrCo_2Cu_3$ to see if the presence of a region with fluctuations close to the critical temperature (T_C) has any effect on the universality class of the ferro-paramagnetic transition. The understanding of this phenomenon allows the development of new magnetic materials,

new devices and new technologies that can have important practical applications.

We begin by identifying the phase transition, and then we present a detailed study of the critical behavior. From the magnetic isotherms measured around the Curie temperature with a relatively small step, we can deduce the Arrott plot. From the shape and the slope of the curves, we can determine the type of the phase transition [37]: if the slope is negative and the Arrott plot close to the Curie temperature have the S shape, the transition from the ferromagnetic state to the paramagnetic state is, therefore, a first-order transition. If the curves have a single inflection point and a positive slope, the transition from the ferromagnetic state to the paramagnetic one is a second-order transition. The positive slope

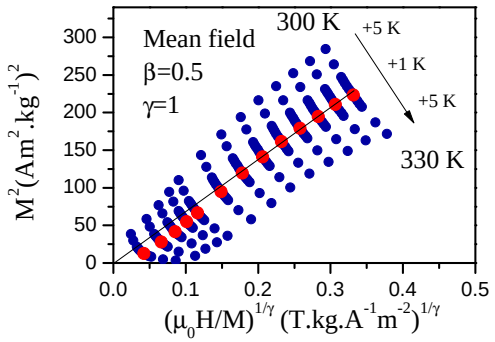

Figure 7. Arrott plot for $PrCo_2Cu_3$. The red circles correspond to the critical isotherm. The black straight line is a linear extrapolation of the critical isotherm in the high field region.

of the isotherms in the high field region depicted in (Fig. 7) clearly indicates that the PM-FM transition is of second order.
Determining the phase transition order is not the only advantage of the Arrott plot. In fact, based on Arrott plot, we can identify:

- **Firstly, χ_0^{-1} and $M_S(T)$ as the intercepts on the H/M axis and positive M^2 axis, respectively.**
- **Secondly, we can easily identify the isotherm which corresponds to Curie temperature and consequently T_C value.**

Arrott plot method assumes that the critical exponents follow mean field theory. Following this method, isotherms plotted in the form of M^2 vs H/M constitute a set of parallel straight lines, and the isotherm at the critical temperature T_C should pass through the origin.

In the case of mean field model Fig. 7 shows that the critical isotherm pass through the origin for $T = 315\,\mathrm{K}$.

In addition, the isotherm plots exhibit some curvature, which calls for more sophisticated analysis. To clarify the nature of magnetic transition phase we have used the modified Arrott plot of $M^{1/\beta}$ vs $(H/M)^{1/\gamma}$ [38]. The modified Arrott plot is given by the Arrott-Noakes equation of state:

$$(H/M)^{1/\gamma} = p\epsilon + qM^{1/\beta} \tag{1}$$

where $\epsilon = (T - T_C)/T_C$ is the reduced temperature, and p and q are constants. Actually, three models have been proposed in literature to determine the modified Arrott plots. These are the 3D-Heisenberg model ($\beta = 0.365$, $\gamma = 1.386$), 3D-Ising model ($\beta = 0.325$,$\gamma = 1.241$), and tricritical mean-field model ($\beta = 0.25$, $\gamma = 1.0$) [39].
The purpose of modifying the Arrott plot is to check if one of the three models can describe the phase transition better than the mean-field model and hereby determine correct values of the critical exponents β, γ and δ. Unfortunately, none of these models can describe the phase transition from the ferromagnetic state to the paramagnetic state. This is obvious because of the isotherm non-linearity observed in Fig. 8.

To find out the appropriate critical exponents β and γ, a rigorous iterative method has been used [40]. Starting from the Mean field model with initial values of β and γ 0.5 and 1, respectively. A linear extrapolation is done from the high-field region which gives $M_S(T)$ and $\chi_0^{-1}(T)$ as an intercept $M^{1/\beta}$ and $(H/M)^{1/\gamma}$ axis, respectively.

A new set of β and γ can be obtained by fitting the data following the Eq. (2) and Eq. (3).

$$M_S(T) = M_S(0)(-\epsilon)^{\beta}, T < T_C \tag{2}$$

$$\chi_0^{-1}(T) = \chi_0^{-1}(0)(\epsilon)^{\gamma}, T > T_C \tag{3}$$

where $M_S(0)$ and $\chi_0^{-1}(0)$ are the critical amplitudes and $\epsilon = (T - T_C)/T_C$ is the reduced temperature [41].

Then a new modified Arrott plot is constructed using the new values of β and γ. As a result, new $M_S(T)$ and $\chi_0^{-1}(T)$ are generated from the linear extrapolation from the high-field region. Consequently, new β and γ can be obtained. This procedure was repeated until the values of β, and γ became unchanged.

Fig. 9 presents the final $M_S(T)$ and $\chi_0^{-1}(T)$ with solid fitting curves. The values of critical exponents β and γ and value of T_C are obtained.

Kouvel-Fisher method is used in order to determine with more precision the values of β and γ [42]:

$$M_S(T)\left(\frac{dM_s(T)}{dT}\right)^{-1} = \frac{T - T_C}{\beta} \tag{4}$$

$$\chi_0^{-1}(T)\left(\frac{d\chi_0^{-1}(T)}{dT}\right)^{-1} = \frac{T - T_C}{\gamma} \tag{5}$$

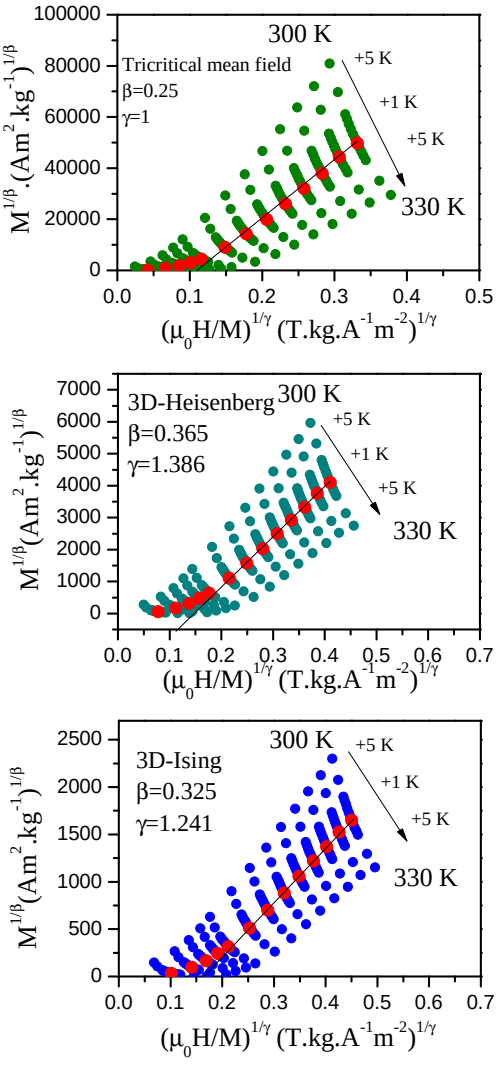

Figure 8. Modified Arrott plots for $PrCo_2Cu_3$. using the tricritical mean field model (top), 3D-Heisenberg model (center) and 3D-Ising model (bottom). The red circles correspond to the critical isotherm. The black straight line is a linear extrapolation of the critical isotherm in the high field region

Based on this method, $M_S(T)\left(\frac{dM_S(T)}{dT}\right)^{-1}$ and $\chi_0^{-1}(T)\left(\frac{d\chi_0^{-1}(T)}{dT}\right)^{-1}$ are a linear functions of temperature with slopes of $1/\gamma$ and $1/\beta$, respectively. They intercept temperature axis for T=T_C. As shown in Fig. 10, the linear fits give β and γ with T_C.

The third exponent δ has been calculated using Widom scaling law as follows [43]:

$$\delta = 1 + \gamma/\beta$$

β and γ values determined from the modified Arrott plot method and Kouvel-Fisher plot were used to deduce δ values.

Furthermore, δ value can be deduced from the fitting

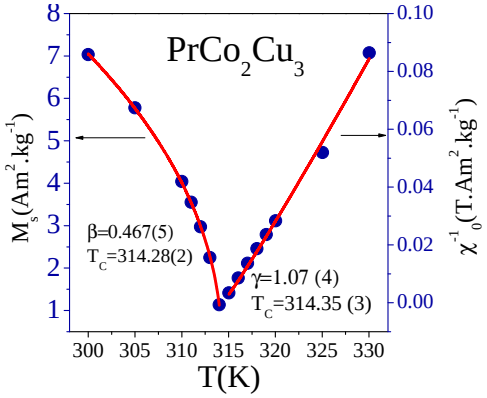

Figure 9. The spontaneous magnetization $M_s(T)$(left) and the inverse of initial susceptibility $\chi_0^{-1}(T)$ (right) plotted against temperature for $PrCo_2Cu_3$. The solid lines represent the fit.

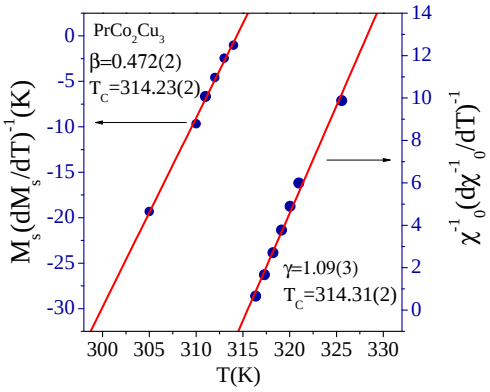

Figure 10. Kouvel-Fisher plots of $M_S(T)/(dM_S(T)/dT)$ (left) and $\chi_0^{-1}(T)/(d\chi_0^{-1}(T)/dT)$ (right) for $PrCo_2Cu_3$. The red solid lines represents the fit

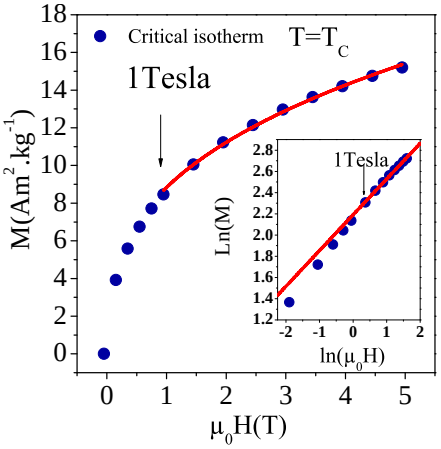

Figure 11. The isothermal magnetization curve against applied magnetic field at T_C for $PrCo_2Cu_3$ sample. The inset shows the same plot in logarithmic scale.

of the critical isotherm using the following equation:

$$M = DH^{1/\delta}, \epsilon = 0, T = T_C \tag{6}$$

Where D is the critical amplitude [41]. Fig. 11 shows the isotherm magnetization $M(H)$ at T $\sim T_C$, with the inset plotted on a log-log scale. δ=3.15(3) was determined based on the fit of the critical isotherm, it is close to the values deduced from the modified Arrott plot and Kouvel-Fisher plot. The critical exponents $PrCo_2Cu_3$ samples are close to critical exponents of mean-field model with a slight deviation.

We verify the validity and the reliability of the founded critical exponents based on the scaling hypothesis:

$$M(H, \epsilon) = \epsilon^{\beta} f_{\pm}(H/\epsilon^{\beta+\gamma}) \tag{7}$$

where f_- for $T < T_C$ and f_+ for $T > T_C$ are the regular functions. By writing magnetization and magnetic field in these renormalized forms, renormalized magnetization $m \equiv \epsilon^{-\beta} M(H, T)$ and renormalized field $h \equiv \epsilon^{-\beta+\gamma} H$, Eq. (7) can be written as:

$$m = f_{\pm}(h) \tag{8}$$

m and h is an important criterion to check the validity of the found critical exponents. Eq. (7) implies that for an appropriate values of β, γ, and δ, we obtain tow universal branches one below Curie temperature and the second above Curie temperature.

Fig. 12 shows that the renormalized isotherms collapse into independent universal branches, which means that the selected critical exponents β, γ, and δ are valid.

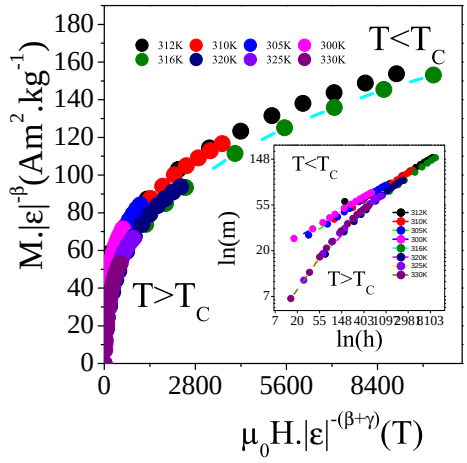

Figure 12. Scaling plots below and above T_C for $PrCo_2Cu_3$ sample. The inset shows the same plot in logarithmic scale.

Based on the results in this section, it is evident that the ferromagnetic (FM) interaction in $PrCo_2Cu_3$ exhibits remarkable properties. First, the estimated exponents are close to those predicted by the mean-field model, albeit with a slight deviation. This suggests that the interaction can be characterized as long-range. However, the slight deviation could possibly be attributed to fluctuations around the spin reorientation that occur prior to the FM-PM transition. Further investigations using DFT and Monte Carlo simulation are needed to fully understand and elucidate this intriguing behavior.

3. *Magnetocaloric effect*

The magnetocaloric effect is a thermodynamic phenomenon that occurs when certain magnetic materials undergo a temperature change in response to a change in magnetic field. Specifically, when the magnetic field applied to a magnetic material is changed, the temperature of that material may increase or decrease, depending on the magnetic properties of the material and the direction of the magnetic field change.

This phenomenon is due to the fact that the magnetization of a magnetic material is related to the entropy of the system, which measures the degree of molecular disorder. Thus, when the magnetic field is changed, the entropy of the system can also change, resulting in a change in temperature.

The magnetocaloric effect is important because it can be used to produce magnetic cooling systems, which are more environmentally friendly and energy efficient than traditional cooling systems.

From the magnetization versus applied magnetic field curves at various temperatures and using the appropriate numerical approximation, it is possible to determine the magnetic entropy change ΔS_M due to a change in the external applied field.

$$\Delta S_{\mathrm{M}} = \mu_0 \int_0^H \left(\frac{\partial M}{\partial T}\right)_H dH$$

Where M is the magnetization, T is the temperature and H is the applied magnetic field. However, if the isothermal $M(H)$ curves are measured by discrete field changes the following expression might be used [44]:

$$|\Delta S_{\mathrm{M}}| = \mu_0 \sum_i \frac{M_i - M_{i+1}}{T_{i+1} - T_i} \Delta H_i$$

Where M_i and M_{i+1} are the initial magnetization at T_i and T_{i+1} temperature respectively when the magnetic field increases by ΔH_i.

In order to show the spin reorientation phenomenon on the $M(H)$ curves more clearly, we have plotted them for the compound $PrCo_3Cu_2$ (see Fig. 13) whose magnetization peak at $T = T_{SR}$ is the sharpest 4).

These features are reflected in the curves of the entropy variation, as shown in the corresponding Fig. 13. We can see a positive peak at T_{SR1} which is related to the spin

Table III. TEC and RCP values of $PrCo_{5-x}Cu_x$ compounds and of other materials for comparison

Compound	$\mu_0\delta H$	ΔS_{max}	RCP	TEC(5 K)	$\frac{TEC}{\Delta\mu_0 H}$	Ref
	T	K	J(K· kg)$^{-1}$	J(K· kg· T)$^{-1}$		
$Pr_{0.5}Er_{0.1}Sr_{0.4}MnO_3$	5	6	360	4.45	0.89	[45]
$Pr_{0.5}Eu_{0.1}Sr_{0.4}MnO_3$	5	5.6	330	4.9	0.98	[45]
$La_{0.8}Na_{0.2}MnO_3$	5	4.8	200	4.6	0.92	[46]
$La_{0.8}Ca_{0.05}Na_{0.15}MnO_3$	5	4.7	188	4.55	0.91	[46]
Ho_2CoMnO_6	7	-	-	6.5	0.928	[47]
$Pr_{1.64}Sm_{0.36}Fe_{17}$	3	3.9	247.26	3.71	1.24	[48]
Pr_2Co_7 (Gd_2Co_7 type structure)	1.5	3.5	103	-	0.928	[49]
Pr_2Co_7 (Ce_2Ni_7 type structure)	1.5	1.1	18.5	-	0.928	[49]
Pr_5Co_{19}	1.5	5	18.2	-	0.928	[50]
Gd_2Fe_2	1.5	0.79	13.3	0.7	0.928	[51]
$GdFe_{1.9}Cu_{0.1}$	1.5	1.2	21.6	-	-	[51]
$GdFe_{1.9}Cu_{0.1}$	1.5	0.9	14.8	-	-	[51]
$HoFe_{0.4}Co_{1.6}$	1.5	0.5	-	-	-	[52]
$HoFe_{0.14}Co_{1.86}$	1.5	1.5	-	-	-	[52]
$ErFe_{0.2}Co_{1.8}$	1.5	1	-	-	-	[53]
$PrCo_3Cu_2$	2	1.15(T_{SR})	43	1	0.5	This work
. $PrCo_{2.5}Cu_{2.5}$	2	1 (T_{SR})	41	1	0.5	This work
$PrCo_2Cu_3$	4	0.5(T_{SR})				
		0.7(T_C)	∼128	-	-	This work

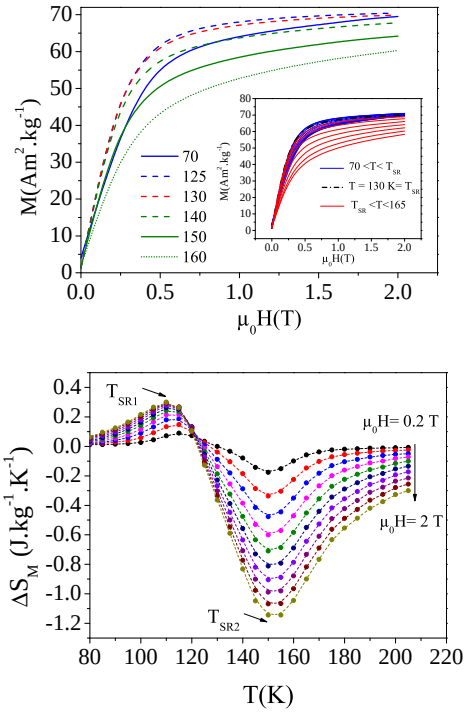

Figure 13. Magnetization $M(\mu_0 H, T)$ curves and magnetic entropy change $\Delta S(T, \mu_0 H)_{\mathrm{M}}$ for $PrCo_3Cu_2$ compound

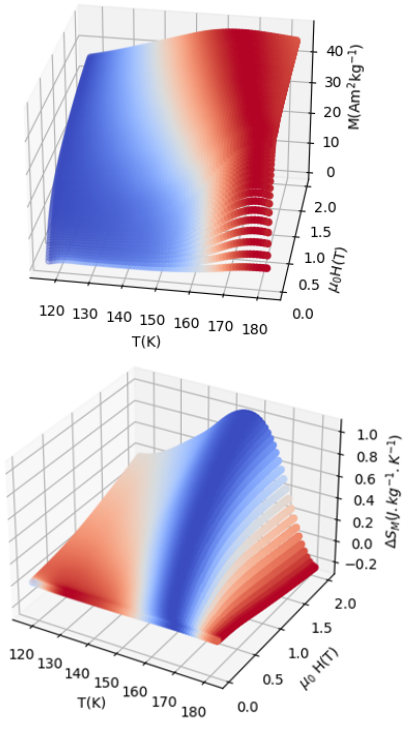

Figure 14. Magnetization $M(\mu_0 H, T)$ curves and magnetic entropy change $\Delta S(T, \mu_0 H)_{\mathrm{M}}$ for $PrCo_2Cu_3$ compound.

reorientation from the plane to the cone, a negative part

at T_{SR2} related to the spin reorientation from the cone

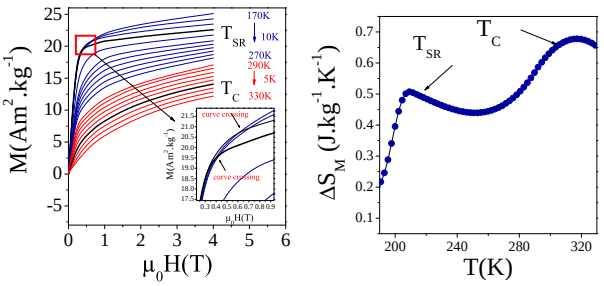

Figure 15. Magnetization $M(\mu_0 H, T)$ curves and magnetic entropy change $\Delta S(T, \mu_0 H)_{\mathrm{M}}$ for $PrCo_{2.5}Cu_{2.5}$ compound

to the axis. Based on the magnetization versus temperature curve of the compound $PrCo_3Cu_2$, the negative and positive peaks are more noticeable for the composition $PrCo_3Cu_2$ as shown in Fig. 13.

Figure. 14 shows typical isothermal magnetization curves for the sample $PrCo_{2.5}Cu_{2.5}$. Note that the low temperature isotherms from 117 K to 182 K show an increase then a decrease of the magnetization value, this is more noticeable at low magnetic field values, this behavior is due to the spin reorientation. For higher temperature values, we found a slight monotonic decrease of the magnetization values, as expected (see Fig. 4). For the compound $PrCo_{2.5}Cu_{2.5}$, we focused on the study of maximum at T_{SR1}, because it is higher than T_{SR2} maximum. This is because the magnetization around the spin reorientation from the planar to the conical arrangement shows a sharper change than that around the ferromagnetic-ferromagnetic transition from the conical to the axial arrangement, as shown in Fig. 4. Now, let's focus on the compound $PrCo_{5-x}Cu_x$ with a copper concentration equal to x=3, in fact the increase of the copper concentration leads to an increase of the spin reorientation temperature and a decrease of the Curie temperature by magnetic dilution, this effect induces a merging of the magnetic entropy around the Curie temperature with that around the spin reorientation temperature T_{SR2}. This results in a huge increase of the width of the entropy variation, the width of ΔS_M exceeds 130 K (see Fig. 15). Moreover, the spin reorientation processes are accompanied by a magnetostriction effect along the c-axis increasing the magnetocaloric potential. In order to evaluate the cooling power around the spin reorientation temperature, we have calculated the figures of merit RCP and TEC, The calculated values are grouped in Tab. III with other compounds for comparison.

IV. CONCLUSION

In conclusion, the results of the Rietveld refinement demonstrate that the $PrCo_{5-x}Cu_x$ compounds are single-phase and crystallize in the $CaCu_5$ structure of the $P6/mmm$ space group. The $3g$ site is identified as the preferred substitution site, and an increase in lattice parameters is observed with the substitution of cobalt by copper. X-ray diffraction on oriented powders reveals that, at room temperature, the anisotropy is axial along the c-axis. Thermomagnetic measurements show that increasing copper concentration in the system leads to a decrease in T_C, while also showing spin reorientation at low temperatures. The spin reorientation temperature increases with higher copper concentrations. The critical exponents adapted for the description of the FM-PM phase transition demonstrate a deviation from the mean field model. Magnetocaloric effect in $PrCo_{5-x}Cu_x$ compounds has been studied, by increasing the copper concentration, it is possible to merge the magnetic entropy variations around T_C and T_{SR}. The spin reorientation phenomenon could be an advantage for the magnetocaloric effect, this effect could be exploited in other materials that show both this phenomenon and a high magnetization.

ACKNOWLEDGMENTS

This work was supported by the National Center for Scientific Research (CNRS), France, and by the "Ministère de l'Enseignement Supérieur et de la Recherche Scientifique" LMOP LR99ES17 Laboratory, Tunisia. The authors would like to acknowledge PHC-Utique 21G1408 project for financial support.

[1] J. X. Zhang, L. Bessais, C. Djega Mariadassou, E. Leroy, and A. Percheron Guegan. *Appl. Phys. Lett.*, 80(11):1960–1962, 2002.
[2] M. Murakami. *J. Appl. Phys.*, 101(9):09C522, 2007.
[3] JF Liu, P Vora, MH Walmer, E Kottcamp, SA Bauser, A Higgins, and S Liu. *J. Appl. phys*, 97(10):10H101, 2005.
[4] Karl J Strnat. *COBALT, SEPT. 1967,–36–, 133-143*, 1967.
[5] R. Fersi, N. Mliki, L. Bessais, R. Guetari, V. Russie, and M. Cabie. *J. Alloys Compd.*, 522:14–18, 2012.
[6] W Bouzidi, N Mliki, and L Bessais. *J. Magn. Magn. Mater*, 441:566–571, 2017.
[7] L. Yin, Y. Guo, and X. Guo. *J. Magn. Magn*, page 169883, 2022.
[8] A.M. Gabay, X.C. Hu, and G.C. Hadjipanayis. *J. Magn. Magn*, 368:75–81, 2014.
[9] X. Xu, H. Zhang, T. Wang, D. Li, Y.and Zhang, and M. Yue. *J. Alloys Compd.*, 699:262–267, 2017.
[10] WQ. Liu, JH. Zuo, M. Yue, WC. Lv, DT. Zhang, and JX. Zhang. *J. App. Phys*, 109(7):07A731, 2011.

[11] KA. Gschneidner Jr and VK. Pecharsky. *Annu. Rev. Mater. Sci.*, 30(1):387–429, 2000.

[12] L. Bessais, E. Dorolti, and C. Djega-Mariadassou. *Appl. Phys. Lett.*, 87, 2005.

[13] S. Khazzan, N. Mliki, L. Bessais, and C. Djega-Mariadassou. *J. Magn. Magn. Mater.*, 322(2):224–229, 2010.

[14] N. Hosni, K. Zehani, T. Bartoli, L. Bessais, and H. Maghraoui-Meherzi. *J. Alloys Compd.*, 694:1295–1301, 2017.

[15] R. Bensalem, W. Tebib, S. Alleg, J. J. Sunol, L. Bessais, and J. M. Greneche. *J. Alloys Compd.*, 471:24–27, 2009.

[16] A. Hamrita, Y. Slimani, M. K. Ben Salem, E. Hannachi, L. Bessais, F. Ben Azzouz, and M. Ben Salem. *Ceram. int.*, 40:1461–1470, 2014.

[17] K. Zehani, R. Bez, A. Boutahar, E. K. Hlil, H. Lassri, J. Moscovici, N. Mliki, and L. Bessais. *J. Alloys Compd.*, 591:58–64, 2014.

[18] H. Rietveld. *Acta Crystallogr.*, 22:151, 1967.

[19] H. Rietveld. *J. Appl. Crystallogr.*, 2:65, 1969.

[20] J. Rodriguez-Carvajal. *Physica B* , 192:55, 1993.

[21] J. Rodriguez-Carvajal, M. T. Fernandez-Diaz, and J. L. Martinez. *J. Phys.* , 81:210, 2000.

[22] L.Bessais, S. Sab, C. Djega-Mariadassou, NH. Dan, and NX. Phuc. *Phys Rev B*, 70(13):134401, 2004.

[23] C. Djega-Mariadassou, L. Bessais, A. Nandra, and E. Burzo. *Phys. Rev. B*, 68:24406, 2003.

[24] L. Bessais, S. Sab, C. Djega-Mariadassou, N. H. Dan, and N. X. Phuc. *Phys. Rev. B*, 70:134401, 2004.

[25] K. Younsi, V. Russier, and L. Bessais. *J. Appl. Phys.*, 107:083916, 2010.

[26] Qu. Johnson, D.H. Wood, G.S. Smith, and A.E. Ray. *Acta Crys B*, 24(2):274–276, 1968.

[27] G Calestani, N Magnani, A Paoluzi, L Pareti, and C Rizzoli. *Physical Review B*, 68(5):054424, 2003.

[28] R. Guetari, R. Bez, C. B. Cizmas, N. Mliki, and L. Bessais. *J. Alloys Compd.*, 579:156–159, 2013.

[29] S. Khazzan, N. Mliki, and L. Bessais. *J. Appl. Phys.*, 105:103904, 2009.

[30] C. Romero-Muniz, J. J. Ipus, J.S. Blázquez, V. Franco, and A. Conde. *Appl. Phys. Lett.*, 104(25):252405, 2014.

[31] A. K. Pramanik and A. Banerjee. *J. Phys: Condens. Matter*, 20(27):275207, 2008.

[32] K. H. J. Buschow. volume 4, page 44. North-Holland, Amsterdam, north-holland, amsterdam edition, 1988.

[33] E. Burzo, A. Chelkowski, and HR. Kirchmayr. Magnetic properties of metals. *Landolt-Börnstein, Numer. data Funct. relationships Sci. Technol*, pages 1–116, 1990.

[34] Z. W. Li and X. A. H. Morrish. *Phys. Rev. B*, 55:3670–3676, 1997.

[35] Q-N. Qi, YP. Li, and JMD. Coey. *J. Condens. Matter Phys.*, 4(42):8209, 1992.

[36] M.R. Ibarra, L. Morellon, P.A. Algarabel, and O. Moze. *Phys. Rev B*, 44(17):9368, 1991.

[37] B.K Banerjee. *Physics letters*, 12(1):16–17, 1964.

[38] A. Arrott and J.E. Noakes. *Phys. Rev. Lett.*, 19(14):786, 1967.

[39] S. N. Kaul. *J. Magn. Magn. Mater.*, 53(1-2):5–53, 1985.

[40] A.K. Pramanik and A. Banerjee. *Phys. Rev. B*, 79(21):214426, 2009.

[41] M. E. Fisher. *Rep. Prog. Phys.*, 30(2):615, 1967.

[42] M. E. Michael J.S. Kouvel. *Phys. Rev*, 136(6A):A1626, 1964.

[43] B. Widom. *J. Chem. Phys*, 43:3892–3897, 1965.

[44] M. Foldeaki, R. Chahine, and T. K. Bose. *J. Appl. Phys.*, 77:3528, 1995.

[45] A. Sakka, R. M'nassri, MM. Nofal, S. Mahjoub, W. Cheikhrouhou-Koubaa, N. Chniba-Boudjada, M. Oumezzine, and A. Cheikhrouhou. *J. Magn. Magn. Mater.*, 514:167158, 2020.

[46] S. Choura-Maatar, M.M. Nofal, R. Mnassri, W. Cheikhrouhou Koubaa, N. Chniba-Boudjada, and A. Cheikhrouhou. *J. Mater. Sci.: Mater. Electron.*, 31:1634–1645, 2020.

[47] D. Mazumdar and I. Das. *J. Appl. Phys.*, 129(6):063901, 2021.

[48] H. Jaballah, W. Bouzidi, R. Fersi, N. Mliki, and L. Bessais. *J. Phys. Chem*, 161:110438, 2021.

[49] R. Fersi, W. Bouzidi, N. Mliki, and L. Bessais. *Intermetallics*, 100:181–187, 2018.

[50] W. Bouzidi, N. Mliki, and L. Bessais. *J. Electron. Mater.*, 47(5):2776–2781, 2018.

[51] M. Saidi, L. Bessais, and M. Jemmali. *J Phys Chem Solids*, 160:110343, 2022.

[52] M. Anikin, E. Tarasov, N. Kudrevatykh, A. Inishev, A. Zinin, A. Teplykh, and A. Pirogov. *Phys. Procedia*, 75:1198–1206, 2015.

[53] X.B. Liu and Z. Altounian. *J. Appl. Phys.*, 103(7):07B304, 2008.